Electronic Supplementary Material (ESI) for Energy & Environmental Science

Electronic Supplementary Information (ESI):

Current Density Dependence of Peroxide Formation in the Li-O_2 Battery and its Effect on Charge

Brian D. Adams, Claudio Radtke, Robert Black, M. Trudeau, K. Zaghib

and Linda F. Nazar

Experimental Details

Preparation of Gas Diffusion Electrodes

The Li^+ form of a perfluorosulfonate ionomer (Li-Nafion) was prepared via a solution-based exchange of the protons in Nafion®.[1] A solution of 0.1 M LiOH was prepared from $LiOH.H_2O$ (>98%, Alfa Aesar). The LiOH solution was added over the course of several hours to a magnetically stirred Nafion® perfluorinated resin solution (5 wt. % in mixture of lower aliphatic alcohols and water, Aldrich). The ion-exchange was deemed to be complete once the pH = 8. This solution typically contained 3.24 wt. % Li-Nafion in water and lower aliphatic alcohols. To eliminate the aqueous-based solvent in this binder, the Li-Nafion solution was mixed with *N*-Methyl-2-pyrrolidone (NMP) (≥99.5 %, Aldrich) at heated to 120 °C. At this temperature, the alcohols and water were completely evaporated and exchanged with NMP as the solvent.

Gas diffusion electrodes were prepared by casting an active (carbon black + binder) layer on a gas diffusion layer. Vulcan XC72 (400 mg), 1 g NMP and 4 g Li-Nafion (10wt%)/NMP were very well mechanically mixed for 10 minutes followed by ultrasonication for 1 hour. Films of this mixture were cast onto Toray carbon paper (TGP-H-030, Fuel Cell Store). After drying at 90 °C for 1 hour, the gas diffusion electrodes were punched from the film (1 cm^2 area) and further dried at 100 °C *in vacuo* for 24 hours. The active layers of these gas diffusion electrodes had an average thickness of 10 µm and masses ranging between 0.5 to 1.5 mg.

Galvanostatic Cycling

Non-aqueous Li–O_2 cells were prepared using a modified Swagelok™ design with 1 M LiTFSI (Novolyte) in dry, distilled TEGDME (<1 ppm H_2O) as the electrolyte. Cells were assembled in an argon filled glovebox with a lithium metal anode, porous separators (millipore glass fiber), and a gas diffusion electrode as the cathode. Electrolyte (50µL) was added to the separator during cell assembly. The cells were purged several times with O_2 (99.994% pure O_2, Airgas,

H_2O < 2 ppm) and subsequently sealed at 1.5 atm. The cells were equilibrated at open circuit for 6 h before testing. The Li–O_2 cells underwent galvanostatic discharge using various current densities to either a lower voltage cutoff of 2.25 V vs. Li/Li^+ or a capacity (mAh) cutoff and charging was cutoff with an upper voltage of 4.7 V.

Electrochemical Impedance Spectroscopy

Impedance measurements were performed using a VMP3 potentiostat/galvanostat with EIS/Z capabilities and EC-Lab® software (Bio-Logic Science Instruments). The DC voltage was maintained at open-circuit and an AC voltage was applied with an amplitude of 5 mV from 300 kHz to 50 mHz.

Electrode Analysis

After electrochemical studies were completed, the cells were disassembled in an Ar-filled glovebox and the electrode was recovered. XRD measurements were carried out using a Bruker D-8 Advance diffractometer employing Cu-Kα radiation (λ = 1.5406 Å). Samples were mounted on a silicon low-background holder and protected from the atmosphere by coating with paraffin oil. SEM samples were prepared in an argon-filled glove box, using a stainless steel holder as the substrate and double-sided carbon tape as the contact point between the sample and the holder. Samples were transferred into the SEM (Zeiss Ultra Plus field emission SEM) under anerobic conditions and images were taken using an accelerating voltage of 5 kV. Electrodes were thoroughly washed with MeCN prior to analysis, and loaded without air exposure.

TEM and EELS analysis was performed with a Hitachi HD2700 STEM equipped with spherical aberration correction (CEOS GmbH) and an EELS spectrometer (Enfina; Gatan). The instrument can provide a resolution of less than 0.10 nm in high-angle annular dark-field mode (HAADF). Films (~ 20 – 40 nm thickness) were prepared from the discharged cathode using focused ion beam (FIB; NB5500) thinning, employing a 40kV Ga ion FIB column providing 3D reconstructions with slicing steps down to 50 nm. The sample was transferred into the TEM chamber without any contact with air.

Note on Current Rates and Capacities

Two units of current rate are often seen in the literature (mA/cm^2 and mA/g_{carbon}) for studies on Li-O_2 batteries. The first metric (mA/cm^2) depends on the electrochemical active surface area (EASA) of the cathode and the latter (mA/g_{carbon}) is highly dependent on the thickness of the oxygen electrode and the relative mass of other components of the electrode. The second has been adapted from other battery systems where the reactions involved are dependent on the bulk of the electrode material, such as intercalation compounds. In this study we use current rates based on the geometric surface area ($\mu A/cm^2$) since the discharge and charging reactions of the Li-O_2 battery are surface reactions, yet the EASA is often very difficult to estimate. In this sense, the unit of $\mu A/cm^2_{geometric}$ is the best for reliable comparison of results with other studies.

Likewise, the units of capacity in studies of the Li-O_2 cell are generally given as mAh/g_{carbon}. This again can give poor comparisons and lead to lack of reproducibility, since the electrochemical reactions occur on the surface. Many other factors such as pore size, thickness, mass and volume of all other components, diameter must all be known if units of mAh/g_{carbon} are to be used and quoted. Here we use values of capacity based again on geometric surface area (mAh/cm^2), displayed as electrical charge transferred since our electrodes all have a geometric surface area of 1 cm^2.

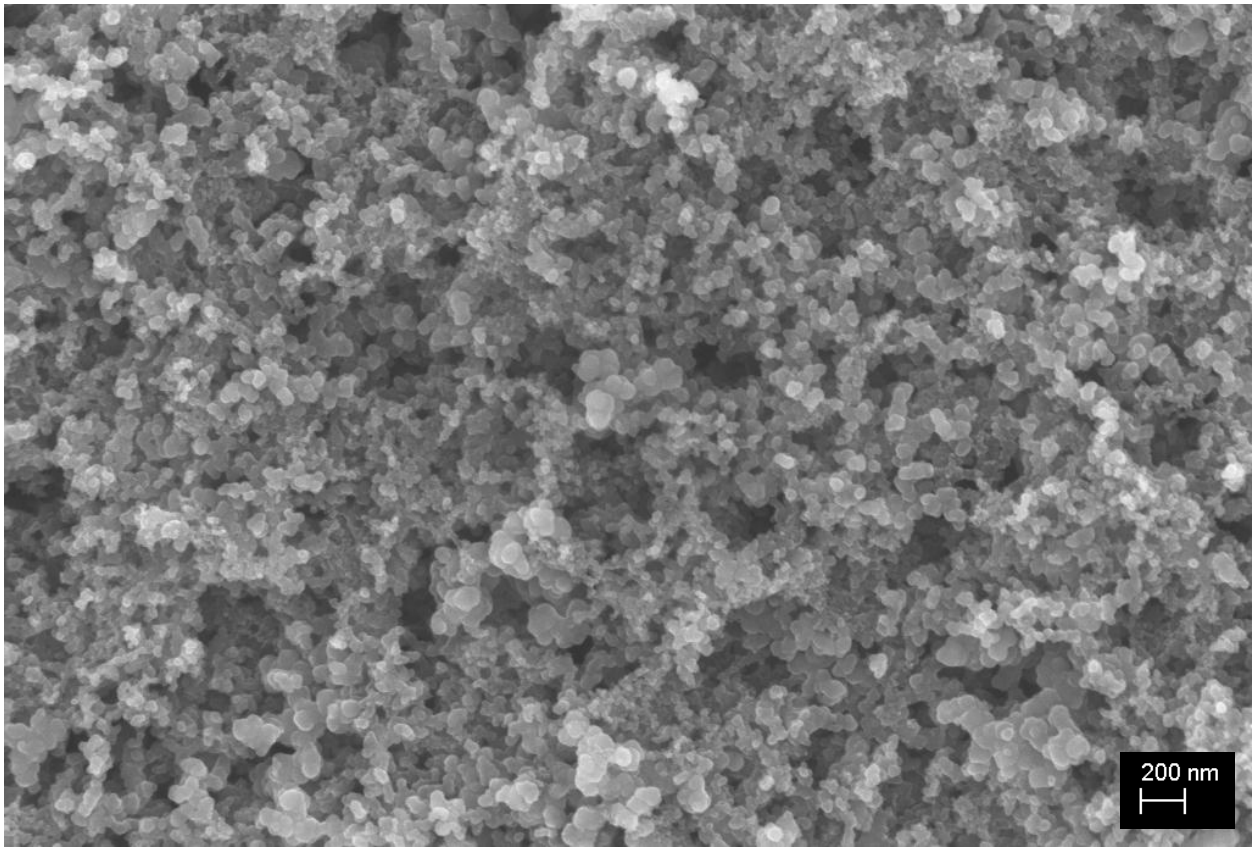

Fig. S1 Full size FESEM image of pristine cathode.

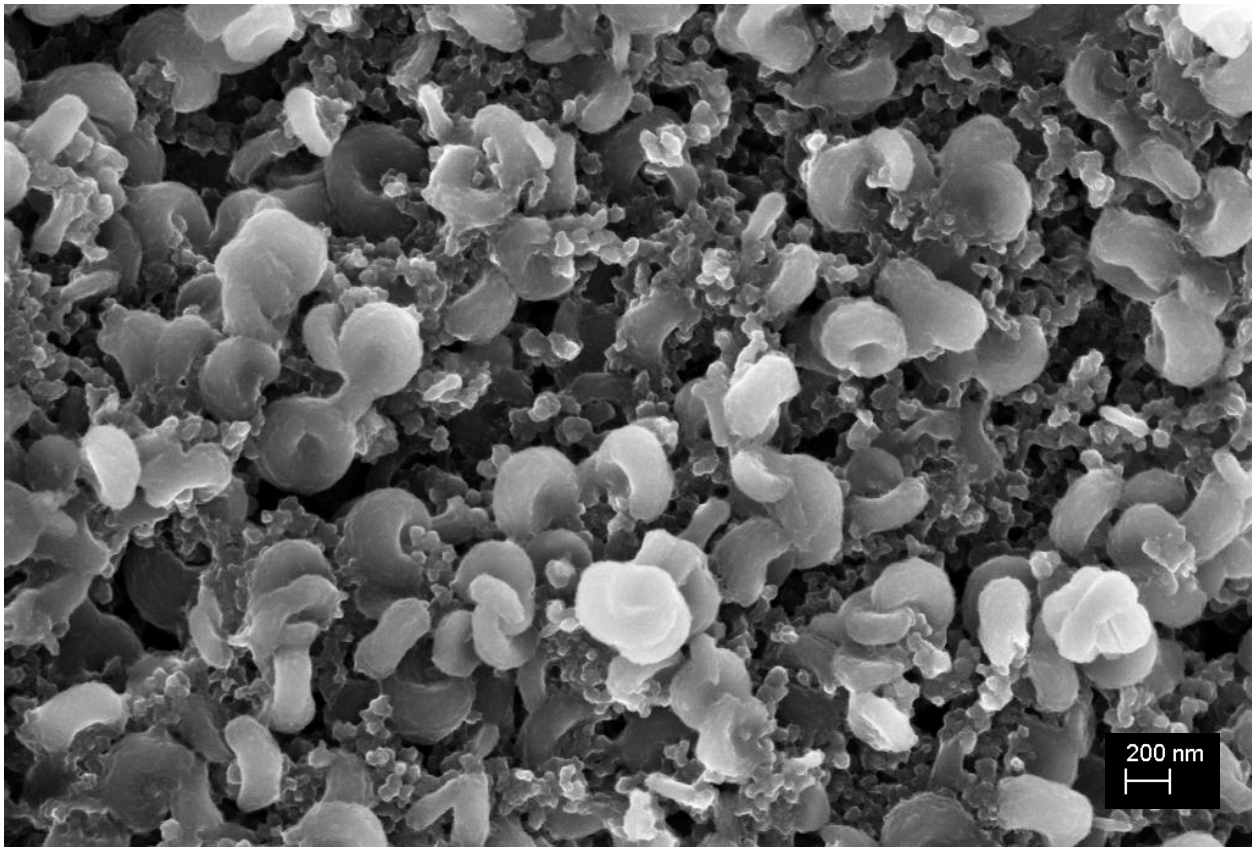

Fig. S2 Full size FESEM image of cathode after discharge at 5 μA/cm^2.

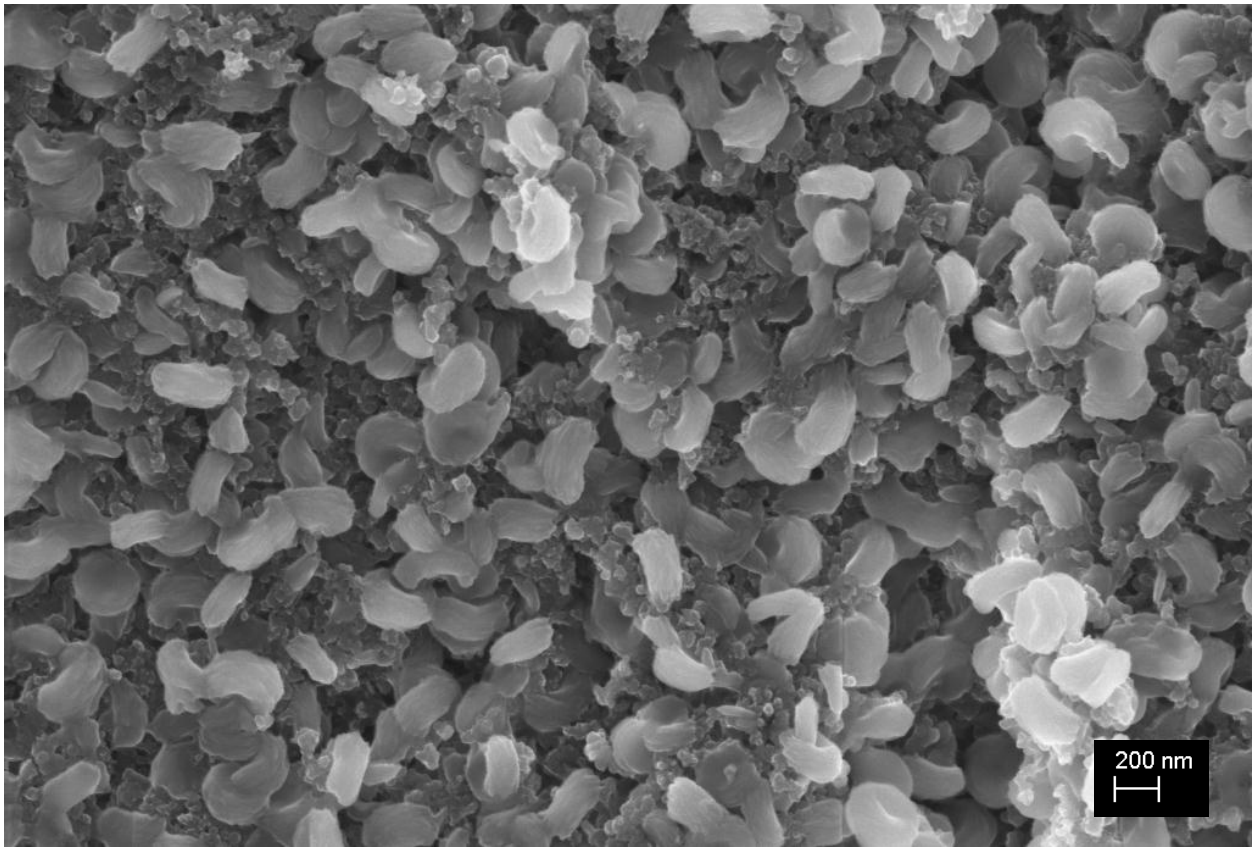

Fig. S3 Full size FESEM image of cathode after discharge at 10 μA/cm^2.

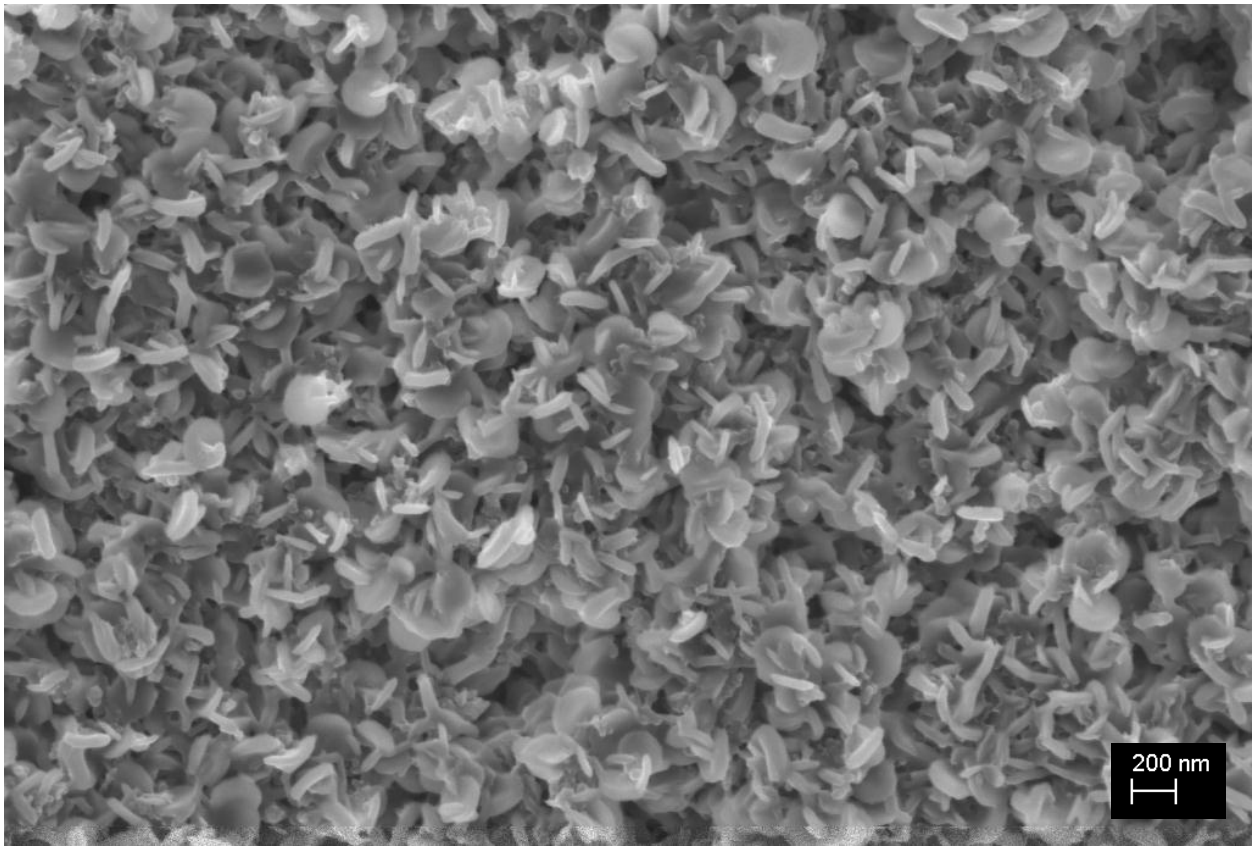

Fig. S4 Full size FESEM image of cathode after discharge at 25 μA/cm^2.

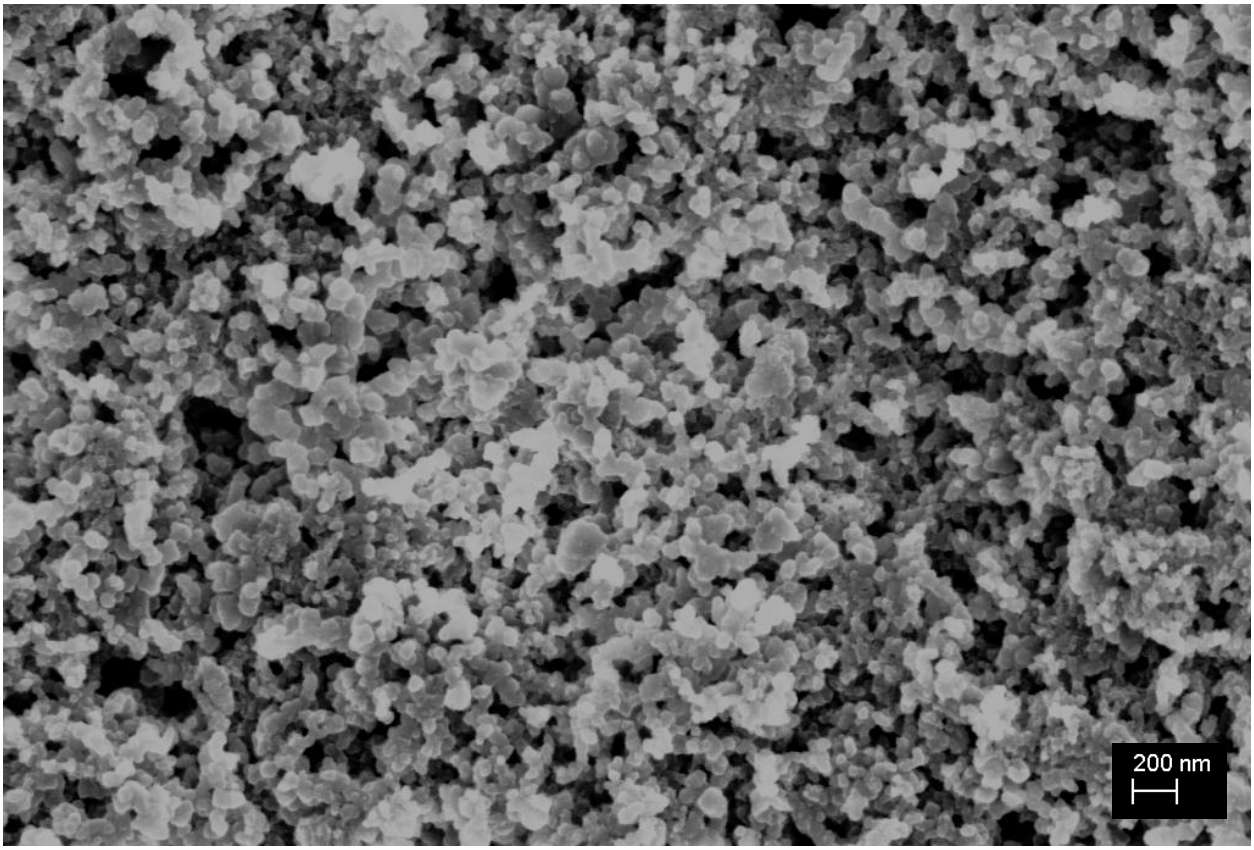

Fig. S5 Full size FESEM image of cathode after discharge at 50 μA/cm^2.

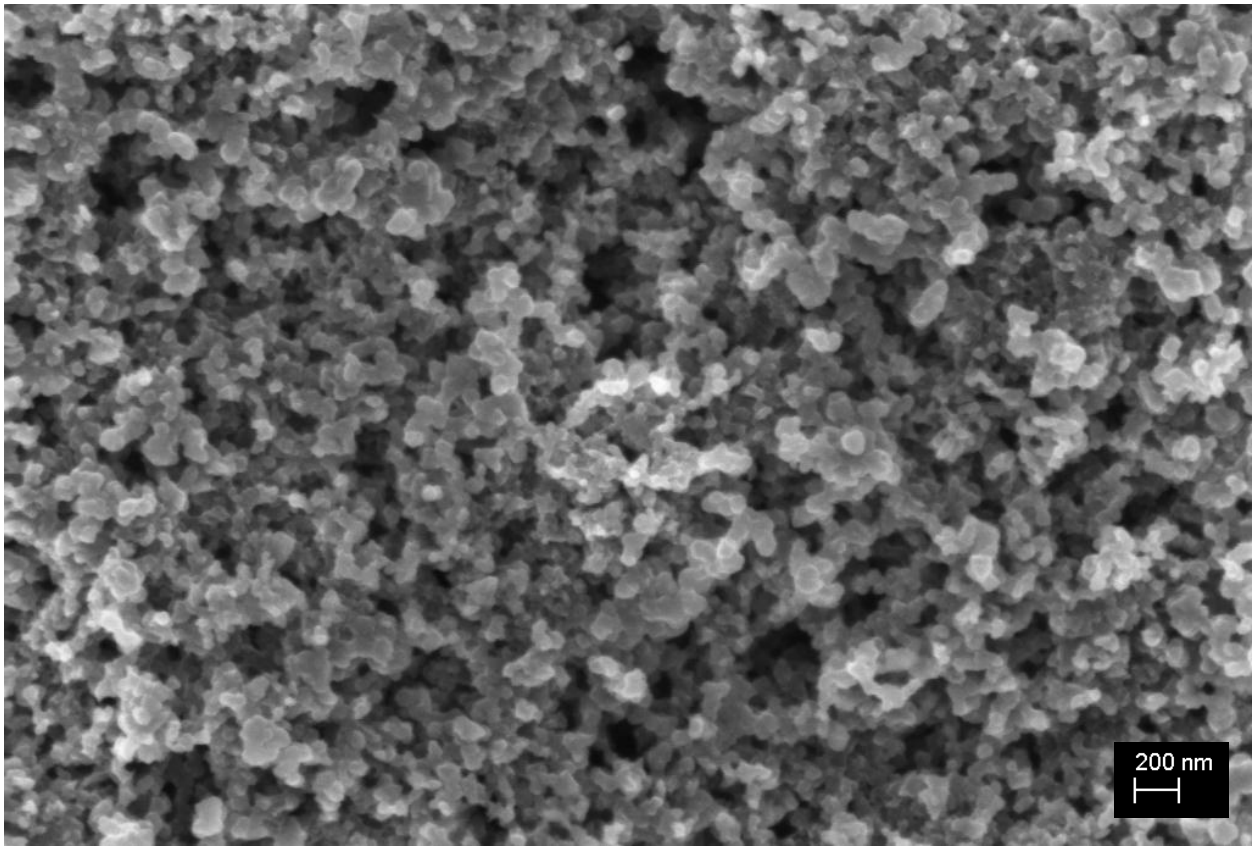

Fig. S6 Full size FESEM image of cathode after discharge at 100 μA/cm^2.

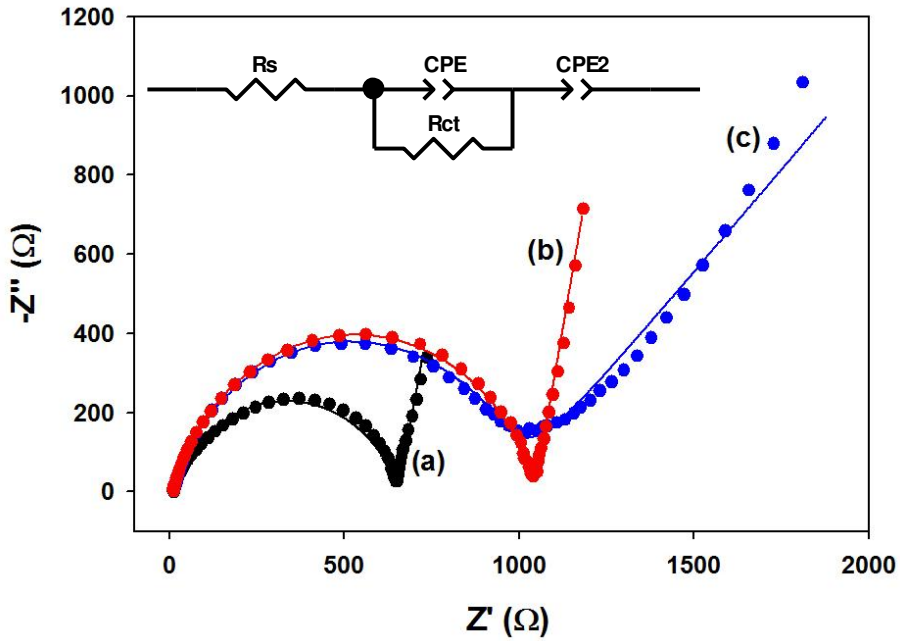

Fig. S7 Nyquist plots of (a) non-discharged cell, (b) cell discharged at 100 μA/cm^2, and (c) cell discharged at 5 μA/cm^2. The inset shows the equivalent circuit that the data (circles) were fitted with (solid lines).

Table S1 Parameters for Figure S7, fitted by the equivalent circuit shown in the inset.

Element	**Non-Discharged**	**Discharged at 5 μA/cm^2**	**Discharged at 100 μA/cm^2**
Rs (Ω)	12.43±1.13%	12.64±0.78%	12.06±0.63%
CPE-T (μF)	6.01±3.53%	3.22±2.46%	2.52±1.70%
CPE-P	0.79±0.46%	0.83±0.34%	0.83±0.21%
Rct (Ω)	643.7±0.68%	955±0.80%	1034±0.34%
CPE2-T (mF)	7.76±4.09%	1.37±1.42%	3.85±1.76%
CPE2-P	0.87±2.95%	0.51±1.69%	0.88±1.26%

The equivalent circuit displayed above in Figure S7 consists of an uncompensated ohmic resistance (Rs) in series with a constant phase element (CPE) in parallel with the charge transfer resistance (Rct). These elements cause the depressed semi-circle shape in the Nyquist plots. At the end of the circuit is a second constant phase element (CPE2), that gives rise to the linear tail following the semi-circle at low frequencies. The uncompensated resistance is roughly the same for each cell and is due to the electronic resistances of the electrodes, contacts, and electrolyte resistance. The constant phase elements defined as CPE(2)-T and CPE(2)-P represent the capacitive contributions of the two electrodes, where the value of CPE(2)-P can range between 0 and 1, with 0 being a pure resistor and 1 being a pure capacitor.

The Rct (or polarization resistance) increases after discharge of the cells at both current rates. Increases of 33% and 38% in Rct relative to the non-discharged cell are observed for the cells discharged at 5 $\mu A/cm^2$ (toroid morphology) and 100 $\mu A/cm^2$ (film morphology), respectively. These similar values provide evidence that the sharp increase in polarization at the end of discharge, which limits the capacity, is governed by the same process at all discharge rates. We can conclude that pore-blocking is not the cause of the polarization, since open pores (void space between carbon particles) are evident in both cases in the SEM images. It is more likely that the polarization is caused by limited mass transport of Li^+ and/or O_2 to the active surface sites by the build-up of Li_2O_2 product. The CPE2 is related to diffusion of active species to the surfaces of the electrodes. The morphology of the discharge product is reflected by this element. The degree of capacitance (CPE2-P) resulting in the linear slope of the Nyquist plot at low frequencies is the same for the discharged cell at high current rate as for the non-discharged cell. This is because the formed Li_2O_2 film of the discharged cell does not significantly change the surface area or morphology of the underlying cathode. However, the CPE2 of the cell discharged at low current rate (Li_2O_2 toroids) has a more resistive character than the others.

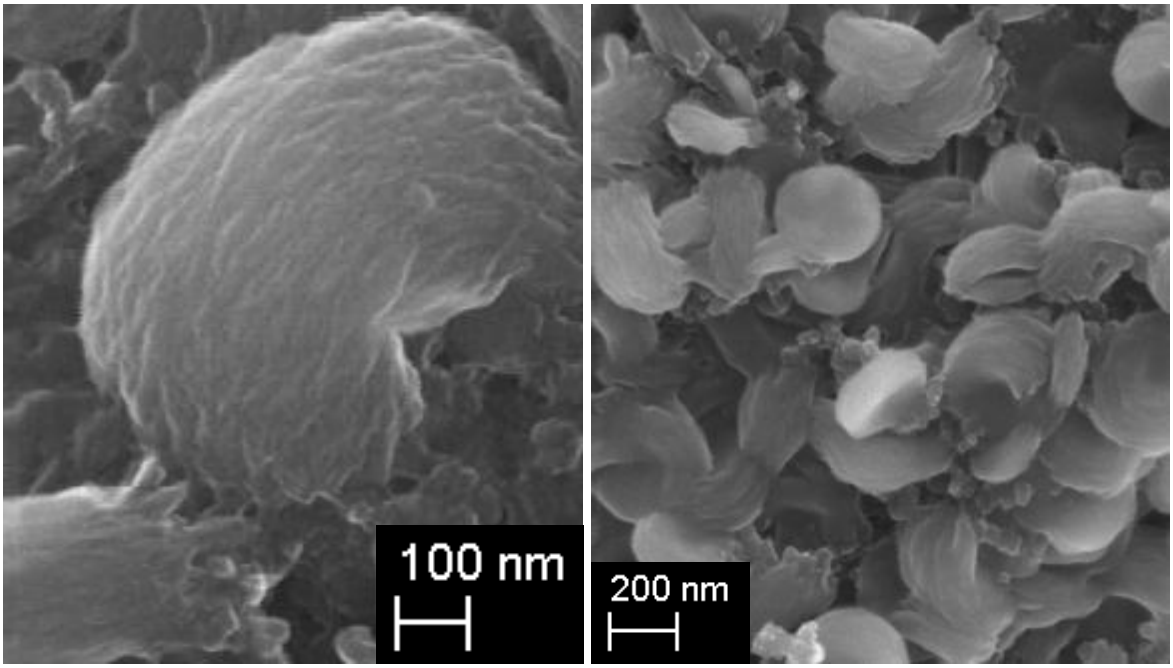

Fig. S8 FESEM images showing the nanocrystallite aggregate structure of the toroids.

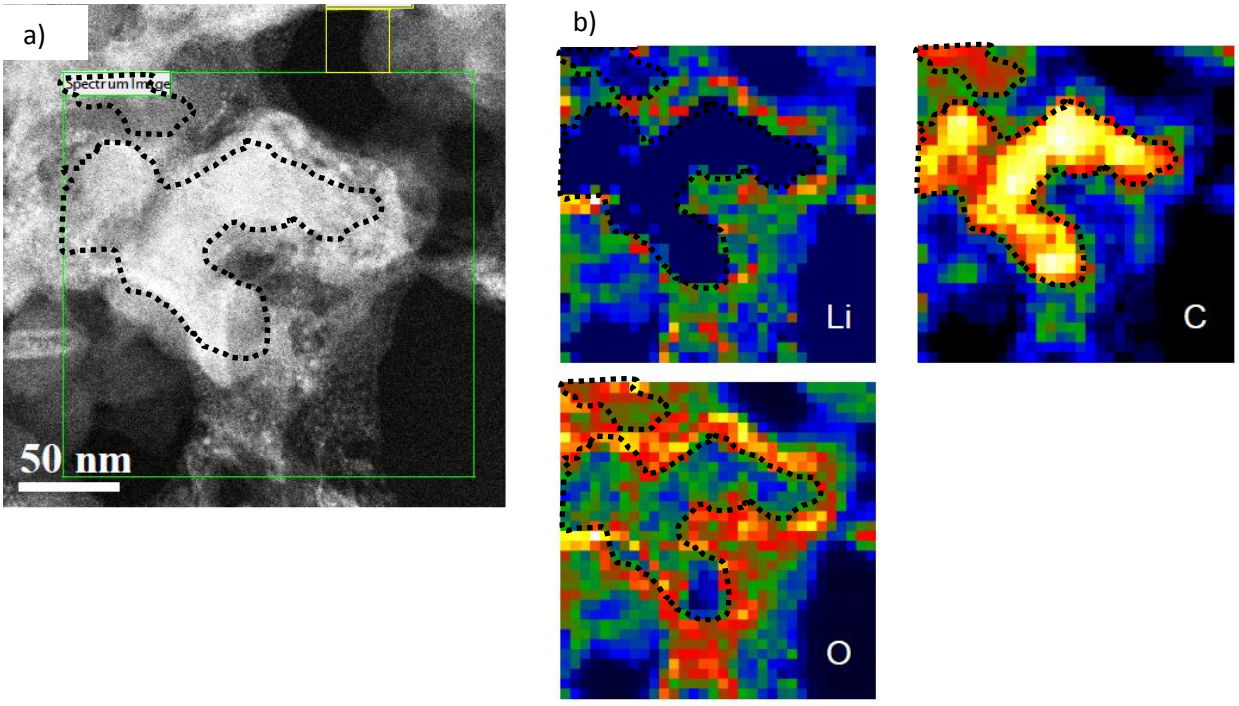

Fig. S9 a) STEM image in high-angle annular dark field mode (HAADF) of a sample section of the electrode material discharged at 50 μA/cm^2 and prepared by focused ion beam bombardment; b) accompanying Li, C and O compositional maps of the area outlined in green in (a) generated by electron energy-loss spectroscopy in the transmission electron microscope (STEM-EELS); these maps are representative of many observations of the electrode. Acquisition time was < 1sec to prevent beam damage to the sample, leading to poor pixellation quality. The dotted black line in all images is the outline from the carbon map, showing the carbon particle.

The images shown above indicate the presence of a ~ 15 - 20 nm thick lithium oxide film around the surface of the carbon. The lithium oxide was extremely beam sensitive, even more so than a crystalline Li_2O_2 reference material prepared in a similar manner, which precluded the acquisition of fast Fourier transform (FFT) images in either case.

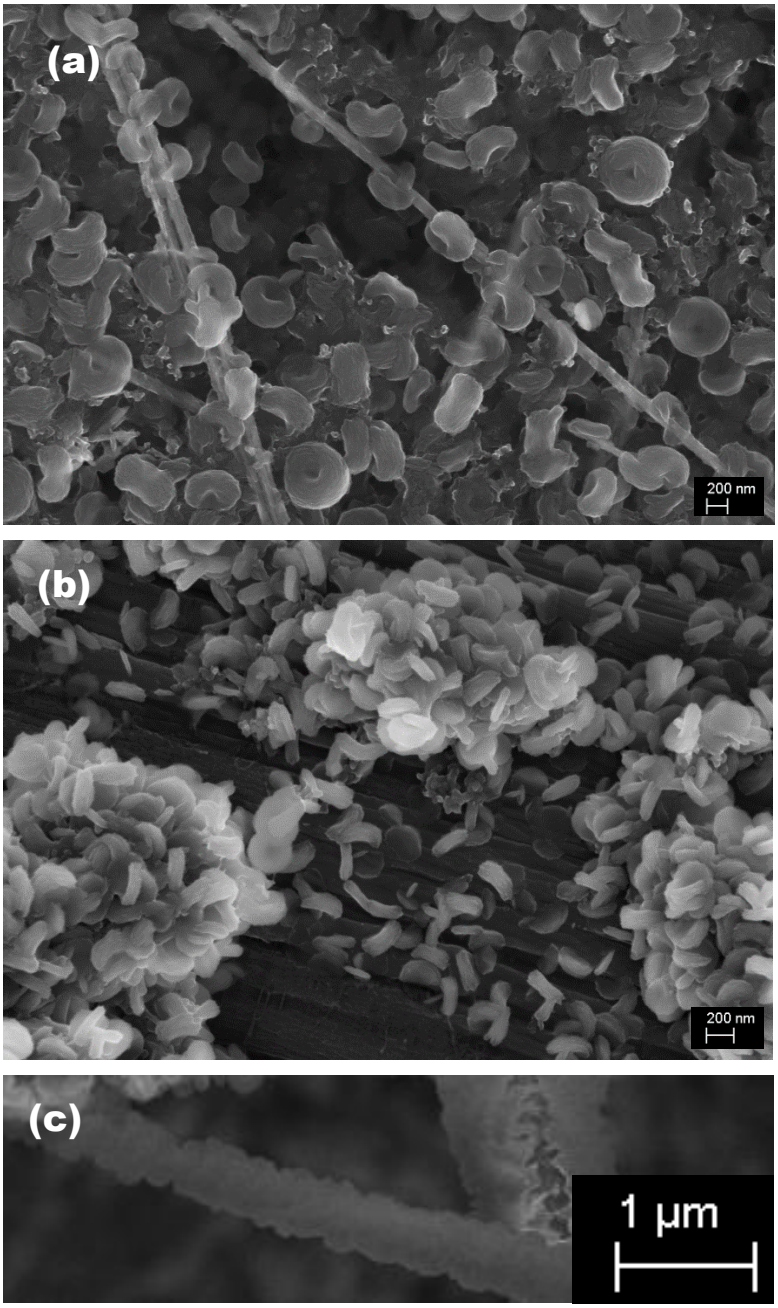

Fig. S10 FESEM images of Li_2O_2 on (a) $Na_{0.44}MnO_2$ nanowires, (b) the Toray carbon paper GDL at a crack in the active carbon coating and (c) a glass fiber from the separator. We note that the bare GDL has negligible capacity (Figure S12). Thus, the Li_2O_2 toroids in (b) *must* have been produced and deposited from the active carbon coating and solution. The glass fiber coated with Li_2O_2 in (c) is from the separator in the cell which adhered to a cathode surface.

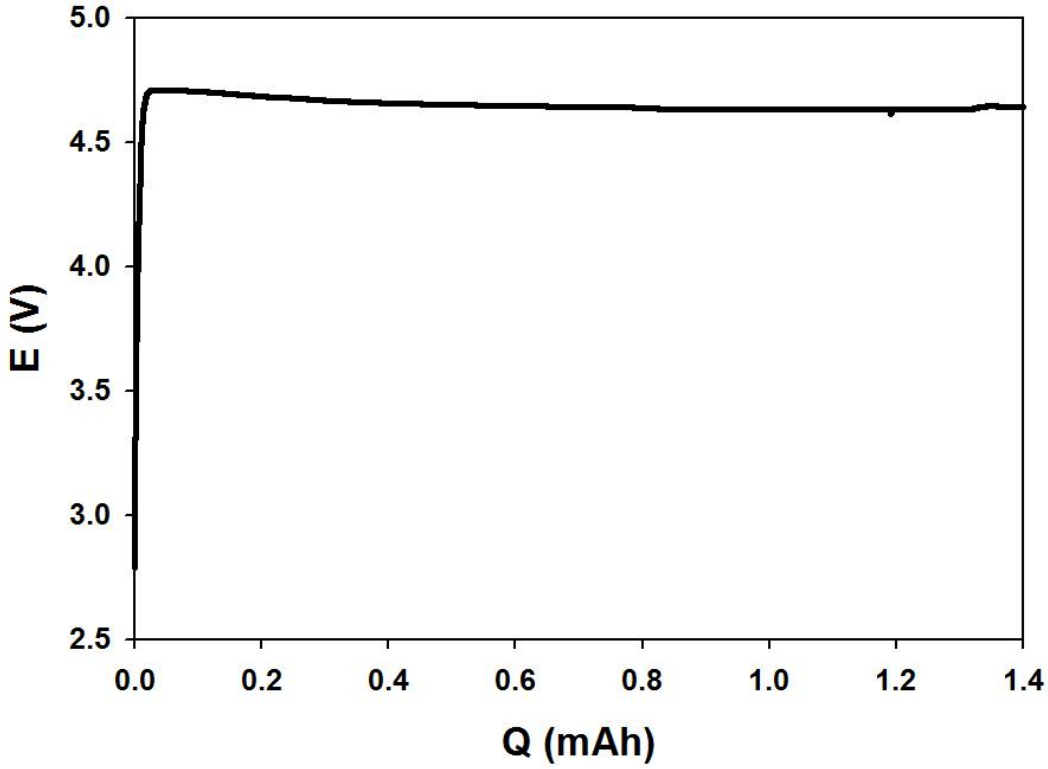

Fig. S11 Charge curve of a pure GDE at 25 μA/cm^2 under O_2 in the absence of peroxide showing that the inherent electrolyte anodic stability limit is at approximately 4.7V.

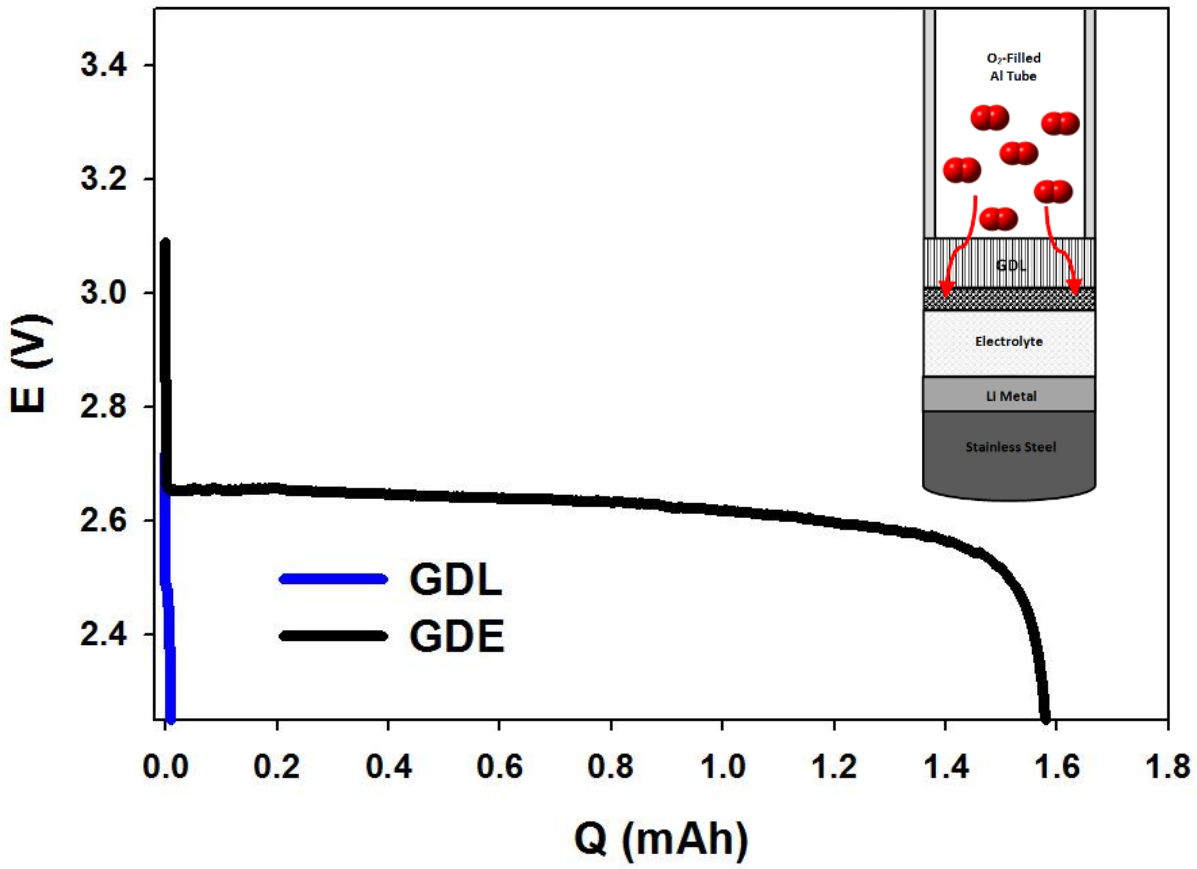

Fig. S12 Discharge curves with gas diffusion layer (GDL) only and gas diffusion layer with an active coating of Vulcan XC72/Li-Nafion (gas diffusion electrode, GDE). Inset: the schematic design of the Li-O_2 cells used in this study. Negligible capacity is observed for the GDL as expected.

References

1 R. R. Garsuch, D.-B. Le, A. Garsuch, J. Li, S. Wang, A. Farooq and J. R. Dahn, *J. Electrochem. Soc.* 2008, **155**, A721.